Desalination and Water Treatment
www.deswater.com
doi: 10.5004/dwt.2020.25876

195 (2020) 275–285
August

Characterization of biosynthesized silver nanoparticles by *Haplophyllum tuberculatum* plant extract under microwave irradiation and detecting their antibacterial activity against some wastewater microbes

Eslam Ibrahim El-Aswar[a,b,*], Seleem El-Sayed Gaber[a], Moustafa Moawad Zahran[b,c], Abdelaleem Hassan Abdelaleem[b]

[a]*Central Laboratories for Environmental Quality Monitoring, National Water Research Center, El-Kanater 13621, Qalyubiyah, Egypt, Tel. +0020242183581/+0020242174665; Fax: +0020242174663; emails: eslam@cleqm.org.eg (E.I. El-Aswar), seleem_gaber@hotmail.com (S. El-Sayed Gaber)*
[b]*Department of Chemistry, Faculty of Science, El-Menoufia University, Shebin El-Kom 32512, Menoufia, Egypt, emails: moustafazahran76@yahoo.com (M.M. Zahran), abdulaleem.h.abdulaleem@gmail.com (A.H. Abdulaleem)*
[c]*Menoufia Company for Water and Wastewater, Holding Company for Water and Wastewater, Cairo, Egypt*

Received 12 June 2019; Accepted 23 March 2020

ABSTRACT

Silver nanoparticles (AgNPs) were successfully fabricated by utilizing $AgNO_3$ as a metal precursor and aqueous extract of *Haplophyllum tuberculatum* extract (HTE) as a source of bioreducing and capping agents through controllable microwave irradiation. Influence of different parameters including pH, HTE volume, silver nitrate concentration, incubation time, and temperature were also discussed. The morphological characteristics were investigated using high resolution transmission electron microscopy, energy-dispersive X-ray spectroscopy, and X-ray diffraction, while the functional groups of bioreducing agents and their efficacy for nanoparticles stabilization were determined using Fourier transform infrared spectroscopy and zeta potential, respectively. Electrochemical behavior of the nanoparticles was studied using cyclic voltammetry (CV) while the optical features were determined using ultraviolet-visible and fluorescence emission spectroscopy. The results indicated that the nanoparticles are semispherical with an average size of 40 nm. These particles have considerable stability confirmed by zeta potential value (–45 mV) and also electrochemically detected at 424 mV. On the other hand, the nanoparticles showed antibacterial activity against total and fecal coliform bacteria. Also, the antibacterial activity of biosynthesized AgNPs against *Staphylococcus aureus*, *Bacillus subtilis*, *Escherichia coli*, and *Klebsiella pneumoniae* was evaluated. Overall, our biosynthesized AgNPs could be used in developing the treatment techniques of wastewater.

Keywords: Nanostructures; Green chemistry; Zeta potential; Wastewater treatment

1. Introduction

Nanochemistry is a promising arena that has a prominent influence on tomorrow's world. It deals with the design, synthesis, and modification of nanostructures that have a size ranges from 1 to 100 nm. The enhanced features of nanostructures make them a good candidate for a variety of applications including catalysis, biosensing, and energy conversion in addition to water treatment [1–3]. Nanostructures synthesis could be prepared through laser mediated fabrication, sonochemical, and thermal decomposition techniques [3–5]. These techniques are known for

* Corresponding author.

their various disadvantages resulting from the hazardous chemicals including the used solvents and reducing compounds, and the produced byproducts [6]. Also, these physicochemical pathways require complicated provisions and high costs due to high energy consumption. So, there is an urgent necessity to find new techniques for the fabrication of nanostructures. Biological techniques are regarded as the most suitable alternatives for the physicochemical techniques because they are simple, cheap, and environmentally benign without the need to use hazardous compounds [5–7]. Biological sources including enzymes, algae, fungi, proteins, bacteria, and plants have been used for metal-based nanostructures fabrication. Synthesis of metallic nanostructures through using plants is more favorable due to the elimination of toxic chemicals and high-energy [8–11]. Plants are rich in numerous biomolecules such as flavonoids, tannins, proteins, and polysaccharides that are capable of the metallic nanoparticles formation and stabilization. Also, they are obtainable, vastly distributed, and appropriate to be used on a large scale [12]. The exact mechanism of nanoparticle synthesis process is still unclear. Various published reports refer to the plant active ingredients as effective reducing and capping molecules in nanoparticle fabrication [11–13]. Some reports showed that the plant biomolecules affect the shape and size of metallic nanostructures. *Magnolia Kobus*, *Cinnamomum camphora*, *Cassica fistula*, *Sorbus aucuparia*, and *Parthenium hysterophorus* were utilized previously for metallic nanostructures synthesis [14 and references are therein]. Various physiological conditions such as temperature, pH, the concentration of precursor ions, plant extract quantity, and reaction time showed an impact on the size, dispersity, and synthesis rate of AgNPs. Vimala et al. [15] found the optimal proportion of reaction mixture for better AgNPs fabrication was fixed as 95 mL 1 mM metal salt with 5 mL of the plant extracts [16]. Pure water that is free of toxic compounds and microbes is necessary for living organisms especially humans. Freshwater sources are reduced due to droughts and population growth [17]. Basically, the most important threat that affects the purity of drinking water is the antimicrobial infection that leads to diseases such as cholera, cryptosporidiosis, and gastroenteritis. Recently, nanochemistry has been used as an efficient tool for water treatment. Silver has been known for its efficient antibacterial properties but the mechanism and the mode of action are still enigmatic [18–20]. In our study, we represent the microwave assisted synthesis of silver nanoparticles (AgNPs) using *Haplophyllum tuberculatum* extract (HTE). The spectral and electrochemical features of biosynthesized AgNPs were studied. The antibacterial activity of the biosynthesized AgNPs has been also investigated.

2. Materials and methods

2.1. Plant collection and extraction process

Plant materials were gathered during summer 2018 and recognized by the botany department of Menoufia University. The plant materials were washed by distilled water to detach the fine dust particles then dried and powdered. A mix of four grams of powdered plant and 250 mL of distilled water was heated at 55°C for 35 min using a water bath. HTE was filtered to eliminate the insoluble plant biomass. The resulted yellow color filtrate was stored in the refrigerator for further studies.

2.2. Silver nanoparticles synthesis

Plant extract was added to silver nitrate ($AgNO_3$; 99.8%, Cambrian chemicals, Canada) then kept in a microwave (MG-2312W, LG Co., Seol, Korea) at a constant power and exposure time of 800 W and 180 s, respectively. A yellowish-brown colloidal suspension from AgNPs was produced then purified through centrifugation (18,000 rpm, 10 min).

2.3. Characterization of the biosynthesized silver nanoparticles

The absorption peak corresponding to surface plasmon resonance (SPR) of the AgNPs suspension was determined using UV-Vis spectrophotometer (Model-SHIMADZU UV-2450, Japan). A diluted nanoparticle suspension was used for UV-Vis analysis at the wavelength range of 200–800 nm. High resolution transmission electron microscopy (HRTEM) (JEM-2100 electronic microscope, JEOL, Japan) was used to evaluate the size and morphology of AgNPs at an accelerating voltage of 300 kV. The crystal nature of biosynthesized AgNPs was characterized using X-ray diffraction (XRD) (D/MAX-IIIC, Rigaku Corporation, Japan). The biomolecules of HTE resulted in metallic nanoparticles biosynthesis was determined using Fourier transform-infrared (FT-IR) spectroscopy. AgNPs were mixed with potassium bromide crystal wafers then dried before examination. FTIR (IR 100/IR 200 spectrometer, USA) analysis was carried out in the range of 4,000–400 cm^{-1}. The fluorescence emission of the excited electron of AgNPs was studied using spectrophotometer (Model-SHIMADZU RF-5301 PC, Japan). A diluted AgNPs sample was subjected to the apparatus using quartz cell at the wavelength range of 200–800 nm.

2.4. Stability studies of biosynthesized AgNPs

The stability of the AgNPs was determined by using zeta potential analyzer (Zeta PALs, Brookhaven, USA). A small volume of the purified AgNPs was taken on the cuvette then subjected to the zeta potential analyzer.

2.5. Electrochemical studies

The electrochemical properties of the nanoparticles were determined using MF-9002 BASi Epsilon potentiostat. The cyclic voltammetry (CV), a potentiodynamic electrochemical technique, was performed using the three-electrode system. A platinum wire, saturated silver/silver chloride electrode, and glassy carbon electrode were used as an auxiliary, reference electrode, and working electrode, respectively. The supporting electrolyte used in the analysis was 0.1 M Phosphate buffer solution (Sigma-Aldrich, USA) of pH 7.8. The glassy carbon electrode was polished then ultrasonicated for 3 min in deionized water. Two milliliters of AgNPs suspension were mixed with 8 mL of Phosphate buffer solution. The dissolved oxygen was removed through purging N_2 gas for 5 min. Cyclic voltammogram was obtained at 100 mV/s scan rate in the potential range of –1.2 to 1.2 V.

2.6. Antibacterial activity

The antibacterial effect of AgNPs was tested against bacterial species in sewage obtained from El-Rahawy drainage, Egypt (30°12 N; 31°02 E). The sewage was treated with AgNPs to examine their antibacterial activity. 0.25, 0.5, and 10 mg AgNPs concentrations were mixed with 250 mL of sewage then shacked at 150 rpm and plated after 2 and 4 h on nutrient agar medium to examine bacterial reduction. The Petri plates were incubated in dark at 44°C and 35°C for fecal and total coliform, respectively. Disk diffusion method was used to determine the antibacterial efficacy of AgNPs against *B. subtilis* and *S. aureus* as gram positive alongside *K. pneumoniae* and *E. coli* as gram negative [21]. Bacterial strain of each species was swabbed on the Muller Hinton Agar onto individual plates. Three discs of Whatman filter paper No. 40 were prepared with 7 mm diameter. Same amounts (30 μL) of the plant extract, silver nitrate solution and biosynthesized AgNPs were subjected to the discs that have been incubated for 24 h at 37°C then the inhibition zones were checked. Statistical data was performed by SPSS Statistics 24.0 software using one way ANOVA at *p*-value 0.05.

3. Results and discussion

3.1. Biosynthesis of silver nanoparticles: a green approach

The predominant technique for AgNPs formation is the reduction of metal precursor ($AgNO_3$). Fabrication of AgNPs through plant extract biomolecules is favored because of their ability to reduce and stabilize the AgNPs. AgNPs were formed after treating 10 mL of HTE with 100 mL $AgNO_3$ solutions (3 mM). The reaction initiated within a few minutes and the reaction mixture color was changed from the yellow color into dark brown representing the AgNPs formation.

3.2. Characterization of the biosynthesized silver nanoparticles

According to the previous studies, the appearance of deep yellowish-brown color is related to SPR produced from pulsing mode coming up during the coupling of electromagnetic filed in visible range with combined vibrations of electrons in conduction band. Fig. 1 shows an absorption band of AgNPs at ~ 442 nm. AgNPs usually exhibit an absorption band in the range of 410 to 450 nm [15,22,23]. UV-Vis spectra of AgNPs resulted from different synthesis conditions, metal precursor and HTE concentration, pH, temperature, and reaction time are provided (Fig. S1). HRTEM images and the histogram of nanoparticles distribution pattern confirm that AgNPs are semispherical with a size range of 15–65 nm (40 nm average size) surrounded by capping layer with about 4 nm thick (Figs. 2a and b). The particle size distribution is shown in Fig. 2c. The energy-dispersive X-ray spectroscopy (EDX) analysis confirmed also the formation of AgNPs (Fig. 2d). The peak around 3.0 keV indicates the presence of silver element [24,25]. The appearance of O peak may be ascribed to X-rays excitation from plant biomolecules containing O related groups which refers to the involvement of the plant biomolecules in capping of AgNPs [26].

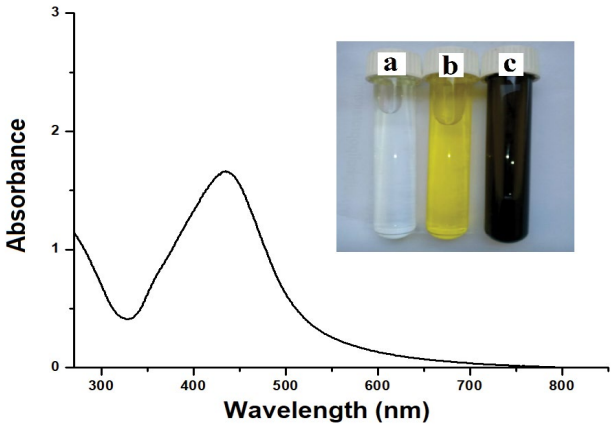

Fig. 1. UV-Vis spectra of biosynthesized AgNPs. The inset indicates the color difference of $AgNO_3$ (a), HTE (b), and AgNPs (c).

The effect of different conditions including silver nitrate concentration, plant extract volume, the reaction pH, and the temperature on the average size of biosynthesized AgNPs was also studied (Fig. 3). Fig. 3a exhibits the different average sizes of AgNPs when different concentrations of $AgNO_3$ solution reacted with 10 mL HTE. In general, the particles size increases with the increase of $AgNO_3$ concentration. At a low concentration of silver nitrate solution, less number of silver cations are available to be reduced by abundant bioreducing molecules and thus the size is relatively small. As the $AgNO_3$ concentration increases, the number of Ag^+ produced increases, and consequently the biosynthesis efficacy is negatively affected resulting in large sized AgNPs. This increase is dependent when the equilibrium between both $AgNO_3$ concentration and bioreducing molecules availability is reached. Therefore, the increase is negligible [15,16]. Fig. 3b shows the average sizes of AgNPs produced from mixing different volumes of plant extract with constant volume (100 mL) of $AgNO_3$ (3 mM) solution. The average size of AgNPs decreases with the increase of added HTE volume. This occurs due to the plenty of bioreducing and stabilizing biomolecules in the medium. However, the average size is relatively steady once equilibrium point is attained as there is no more silver cations available yet [27]. Similar findings were reported earlier [15] where the biogenic AgNPs using *Couroupita guianensis* have shown direct effect on size and biosynthesis rate in accordance with different plant extract. The pH is one of the most significant factors that affect the metal nanoparticles synthesis. At neutral medium, the reaction initiated and AgNPs fabrication was accomplished through 20 min. At acidic medium, AgNPs yield was low with larger sizes of nanoparticles. At basic medium, yield was high with smaller sizes nanoparticles owing to the presence of a sufficient number of functional groups responsible for reduction and stabilization. At pH 12, flocculation of metallic nanoparticles was observed. Fig. 3c infers that the average size of nanoparticles decreases with increasing pH from 5 to 8, but continuous increase in pH causes aggregation. At strong basic solutions, deprotonation of some biomolecules may occur and this gives rise to detaching the stabilizing layer surrounding AgNPs resulting in aggregation

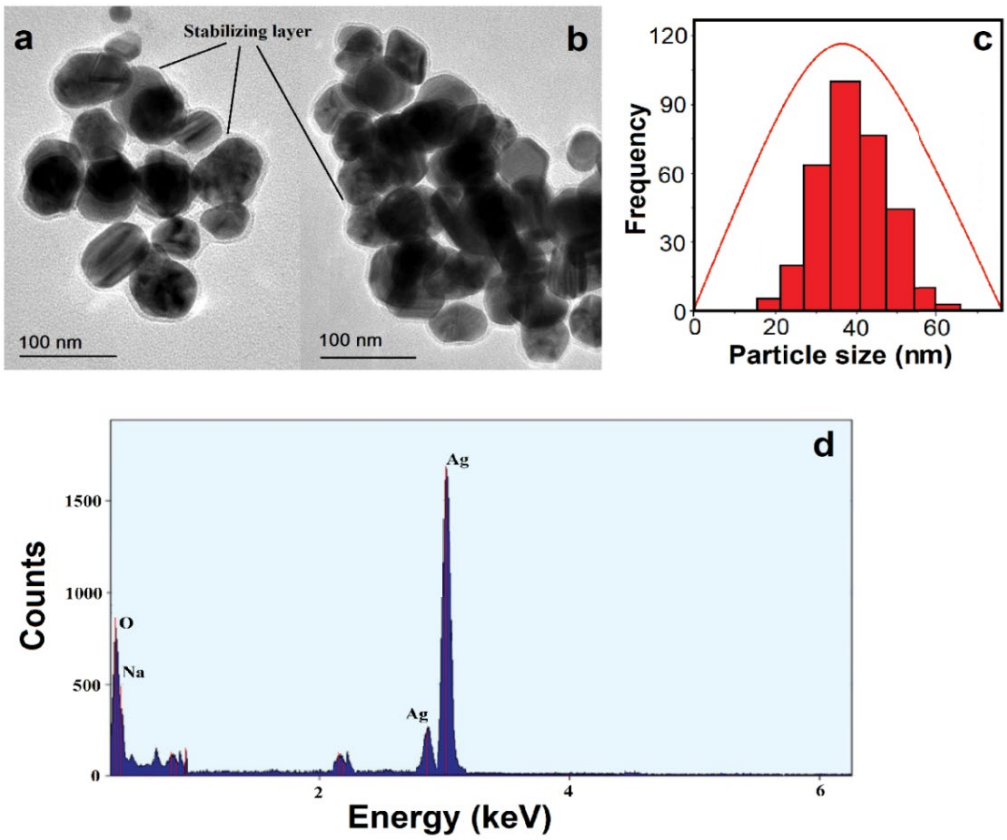

Fig. 2. HRTEM images display biosynthesized AgNPs (a and b), histograms of the size distribution (c), and EDX spectra of biosynthesized AgNPs (d).

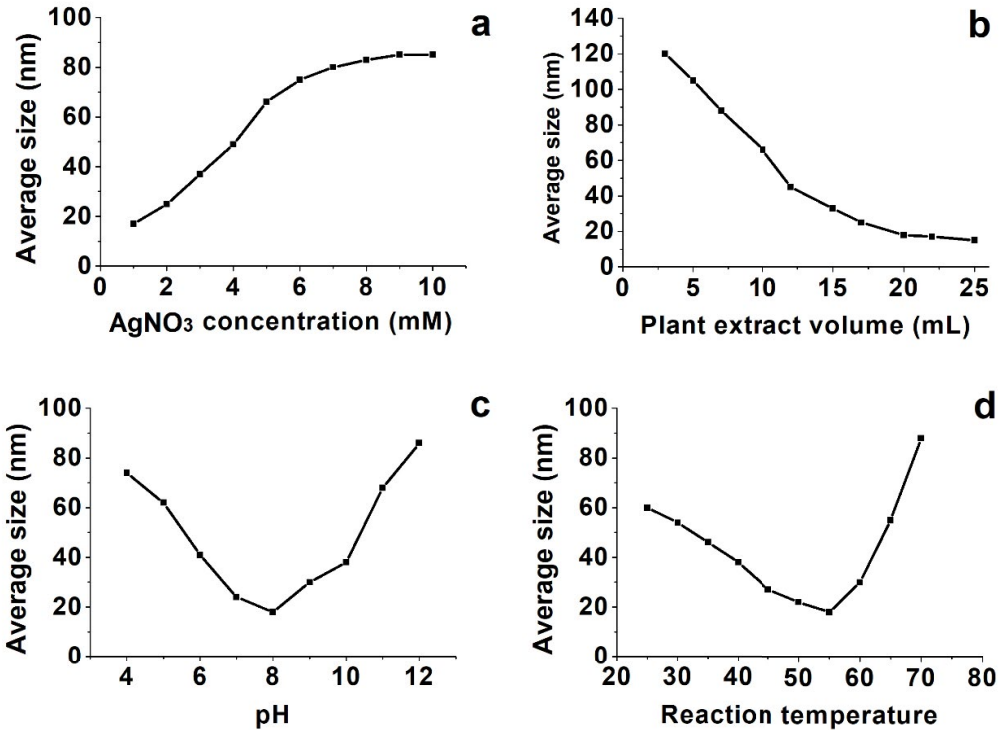

Fig. 3. Effect of (a) $AgNO_3$, (b) plant extract volume, (c) pH, and (d) reaction temperature on nanoparticles size.

and thus larger size nanoparticles [28,29]. Elevating the reaction temperature enhanced AgNPs biosynthesis. While the reaction temperature raised from 30°C to 55°C, the yield increased with comparatively small size of AgNPs. Keep rising the temperature (higher than 55°C) boost the crystals that surround the nucleus leading to larger AgNPs (Fig. 3d) [30].

Fig. 4 shows the XRD pattern of synthesized AgNPs. The observed diffraction peaks at 2θ = 38.13°, 44.30°, 64.34°, and 77.42° were coincided with (111), (200), (220), and (311) diffraction planes, respectively, which designated the cubic crystal structure of AgNPs. The XRD pattern showed that crystalline AgNPs were biosynthesized through the bioreduction of Ag^+ ions by HTE. Similar results were reported in earlier studies [19,31]. The biomolecules with the capability to reduce Ag^+ forming AgNPs (Ag^0) were determined by using FT-IR spectroscopy. Fig. 5 displays the FT-IR spectra of HTE. The absorption bands at 3,555 cm^{-1} corresponds the O–H stretching vibrations [32]. The C–H vibration bands were appeared at 3,065 and 2,925 cm^{-1} while, the observed band at 1,705 cm^{-1} represents the C=O stretching vibrations [33,34]. The bands detected at 1,442 and 1,475 cm^{-1} refer to C–C stretching of aromatics while the 1,085 cm^{-1} band could be attributed to C–O stretching of alcoholic and phenolic compounds [35]. A 585 cm^{-1} band represents the metal-ligand stretching resulted from metal nanoparticles-biomolecules interaction [34,36]. HTE absorption bands exhibits bands that correspond to functional groups of polyphenolics and acids. Also, previous studies confirmed the presence of flavonoids and other phenolic compounds in HTE. These biomolecules act as bioreductant and capping agents [37,38].

The fluorescence emission could be initiated by electrons photoexcitation and subsequent relaxation [39]. Fig. 6 illustrates the fluorescence emission of the AgNPs electrons photoexcited at 380 nm. The fluorescence emission peak was detected at ~469 nm. Our results are agreed with previous published reports [40]. The fluorescence process of metals resulted from electron transfer in the band below the Fermi level to holes in the d bands. The fluorescence emission of AgNPs specifically produced from the transition of electrons from the conduction band ($5sp^1$) to valence levels ($4d^{10}$) [39].

3.3. Stability studies of biosynthesized AgNPs

Stability of metallic nanoparticles could be studied efficiently using zeta potential. The highly stable metal nanoparticles showed zeta potential values over than +30 or –30 mV while, zeta potential values around –15 or +15 mV means that the nanoparticles at the doorstep of agglomeration [41]. Our fabricated AgNPs showed zeta potential of –45 mV (Fig. 7). Owing to the highly negative electrostatic charges on the surface of AgNPs which generate repulsive forces, form high-energy barrier and possibly preserve the AgNPs without affinity to flocculation [42].

3.4. Electrochemical studies

CV is a useful technique to study the electrochemical behavior of different substances. Electrochemical detection of AgNPs was occurred based on the faradaic charge transfer after striking the electrode by AgNPs [43]. AgNPs were oxidized at the glassy carbon working electrode giving

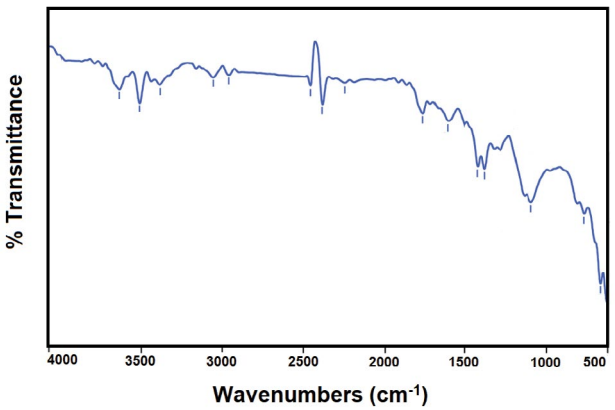

Fig. 5. FTIR spectra of biosynthesized AgNPs with HTE.

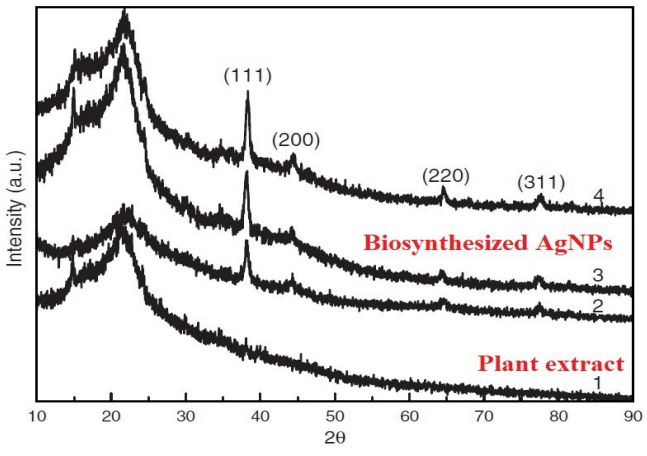

Fig. 4. X-ray diffraction pattern of biosynthesized AgNPs.

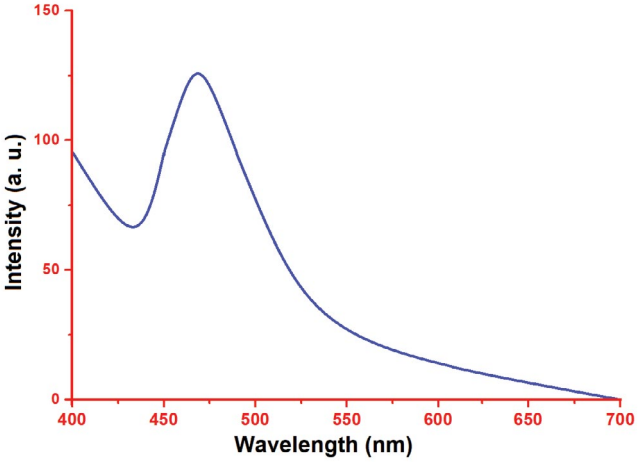

Fig. 6. Fluorescence emission of biosynthesized AgNPs with HTE.

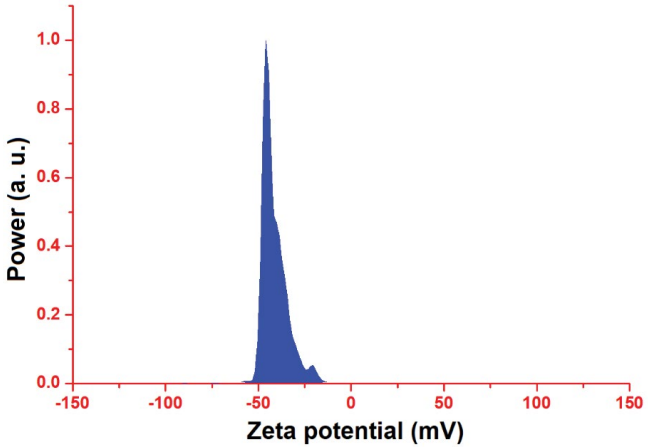

Fig. 7. Zeta potential measurements of biosynthesized AgNPs with HTE.

rise to the anodic peak. Our fabricated AgNPs showed an anodic peak current of 16.54 μA at 424 mV (Fig. 8). AgNPs electrochemical oxidation data of recent published reports confirm our obtained results [44,45].

3.5. Antibacterial activity of AgNPs

The most critical issue afflicting people around the world is water pollution. The main sources of this pollution are industrial wastewater and sewage discharge. However, sewage accommodates mainly all species of non-pathogenic and pathogenic microorganisms which responsible for diseases [46]. In our study, AgNPs were used to determine their antibacterial efficiency against the sewage pathogens. The results showed no bacterial growth in the Petri dishes when the sewage was treated with AgNPs. Increased bacteria population reduction was observed upon increasing both AgNPs concentration and incubation time (Table 1).

In addition, the antibacterial activity of AgNPs against isolated bacteria was studied. The control disks (5 mM silver nitrate and HTE suspension) show no inhibition zones against the chosen strains. Fig. 9 reveals the excellent antibacterial activity of AgNPs manifested by inhibition zones. The statistical analysis exhibited that there was no significant difference among isolated bacteria in the activity of AgNPs with p = 0.734 (Table 2). This antibacterial activity originates from electrostatic interactions between positively charged AgNPs with the overall negatively charged surface of the bacteria which leads to cell death through disruption of transport mechanism [47,48]. AgNPs were observed near the cellular membrane (Figs. 10 and 11). These nanoparticles promote the rupture of a cell membrane, inhibit protein function as well as destruct the DNA [48]. As a result of the cell membrane deterioration alongside the decline of adenosine triphosphate (ATP) level in the bacterial cell, the bacteria eventually will meet its death [49]. Consequently, AgNPs are deemed as a broad-spectrum antibacterial agent [50].

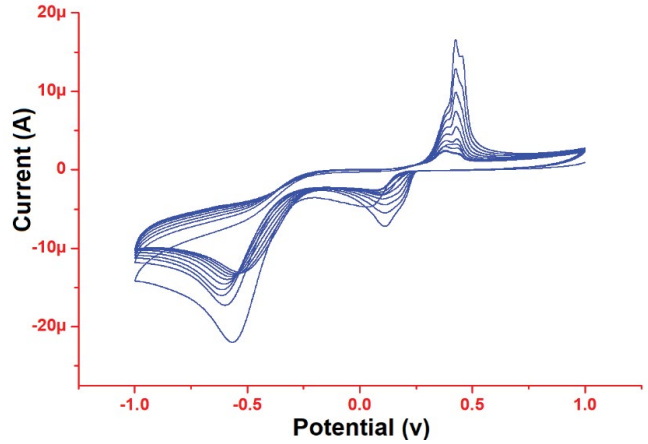

Fig. 8. Cyclic voltammogram of biosynthesized AgNPs with HTE.

4. Conclusion

AgNPs has been synthesized through microwave assisted biosynthesis using HTE plant which is considered as a rapid, simple, green, cost-efficient, and ecofriendly approach. Reaction parameters such as silver nitrate concentration, plant extract volume, the reaction pH, and temperature were investigated to determine their impact on the size of formed particles. AgNPs were characterized

Table 1
Antibacterial activity of biosynthesized AgNPs (A) control after 2 h, (A1–A3) 0.25, 5, 10 mg in 250 mL of sewage, respectively; (B) control after 4 h, (B1–B3) 0.25, 5, 10 mg in 250 mL of sewage, respectively

Code	Total coliform	Fecal coliform
	CFU/100 mL	CFU/100 mL
A (Control)	86×10^4	35×10^4
A1	65×10^2	8×10^2
A2	20×10^2	740
A3	95	60
B (Control)	84×10^4	33×10^4
B1	55×10^2	2×10^2
B2	720	22
B3	40	0

Table 2
Statistical analysis of antibacterial activity of biological AgNPs on isolated bacteria

AgNPs concentration (μg/mL)	Inhibition zone (mean ± SE)	p-value
85	15.75 ± 1.43	
65	14.50 ± 0.86	
45	16.25 ± 2.92	0.734
25	16.00 ± 3.00	
5	12.75 ± 0.75	

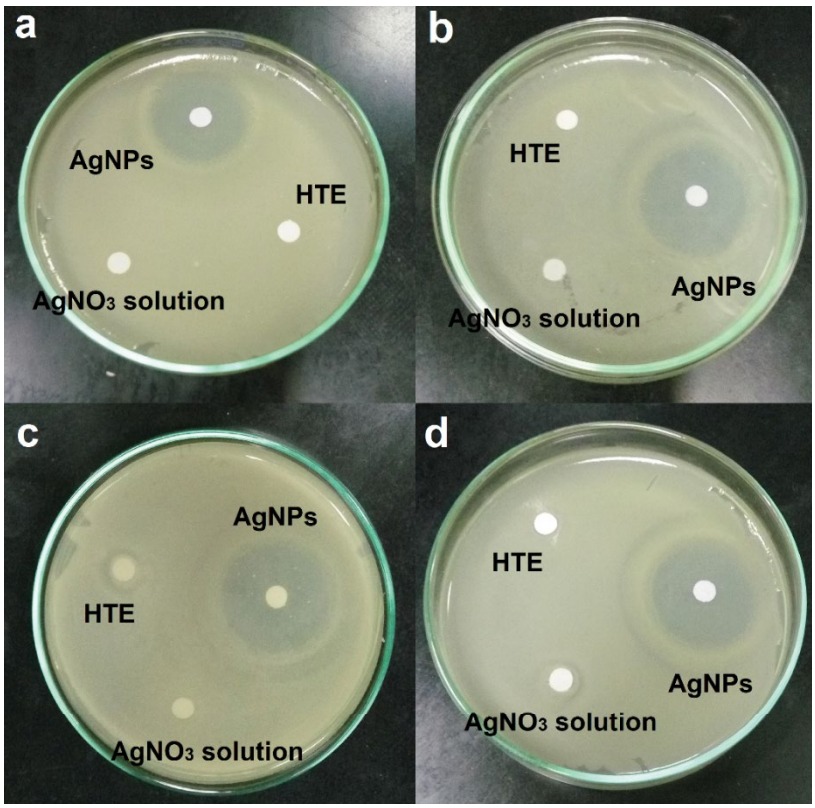

Fig. 9. Photo images how the zone of inhibitions observed for AgNPs action against of (a) *S. aureus*, (b) *B. subtilis*, (c) *E. coli*, and (d) *K. pneumoniae*.

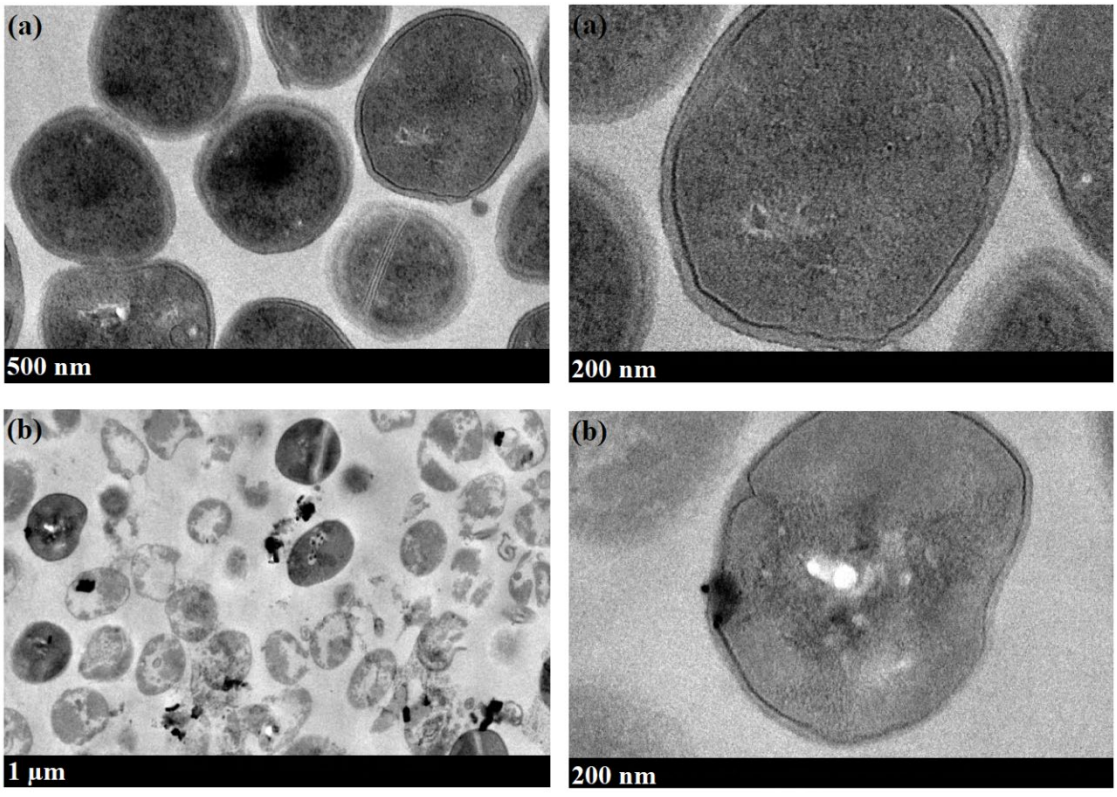

Fig. 10. TEM images of *S. aureus* in the (a) absence and (b) presence of AgNPs on two different scales.

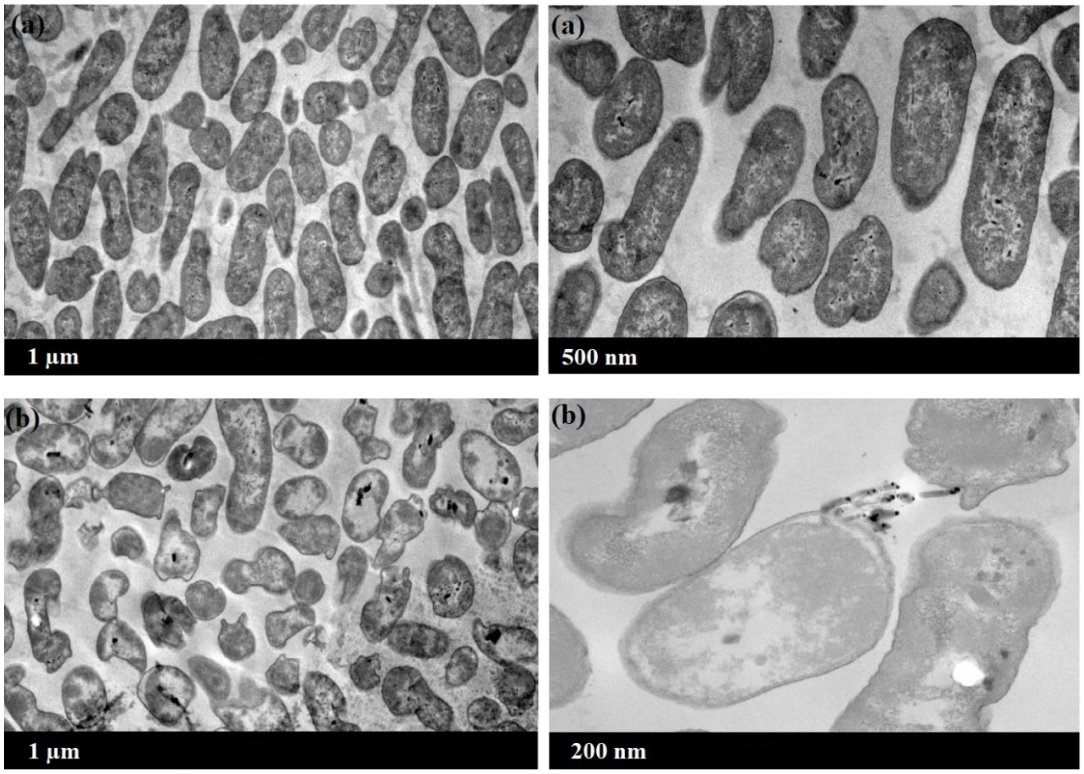

Fig. 11. TEM images of *K. pneumoniae* in the (a) absence and (b) presence of AgNPs on two different scales.

using UV-Vis spectroscopy, HRTEM, fluorescence spectrophotometer, FTIR, zeta potential, and cyclic voltammetry. FTIR studies confirmed the role of polyhydroxy and phenolic biomolecules in the bioreduction along with the capping and stabilizing of AgNPs. HRTEM images determined the morphology of biosynthesized AgNPs. Zeta potential measurements confirmed the high stability of our fabricated nanoparticles. AgNPs antibacterial mechanism against clinically isolated gram positive and gram negative bacteria has been confirmed. Application of our fabricated AgNPs in the treatment of sewage water makes these nanoparticles a promising candidate to replace conventional methods.

Acknowledgment

The author would thank the chemistry department at Menoufia University, Nanotechnology Center at Kafr El-Sheikh and Central Laboratories for Environmental Quality Monitoring (CLEQM), and National Water Research Center (NWRC) for all facilities they offered to complete this work.

References

[1] B. Ankamwar, V. Kamble, U.K. Sur, C. Santra, Spectrophotometric evaluation of surface morphology dependent catalytic activity of biosynthesized silver and gold nanoparticles using UV-vis spectra: a comparative kinetic study, Appl. Surf. Sci., 366 (2016) 275–283.

[2] R.M. Kulkarni, R.S. Malladi, M.S. Hanagadakar, M.R. Doddamani, U.K. Bhat, Ag–TiO_2 nanoparticles for photocatalytic degradation of lomefloxacin, Desal. Water Treat., 57 (2016) 16111–16118.

[3] M. Zahran, A.H. Marei, Innovative natural polymer metal nanocomposites and their antimicrobial activity, Int. J. Biol. Macromol., 136 (2019) 586–96.

[4] Y. Li, Q. Qiang, X. Zheng, Z. Wang, Controllable electrochemical synthesis of Ag nanoparticles in ionic liquid microemulsions, Electrochem. Commun., 58 (2015) 41–45.

[5] A.M. Shanmugharaj, S.H. Ryu, Excellent electrochemical performance of graphene-silver nanoparticle hybrids prepared using a microwave spark assistance process, Electrochim. Acta, 74 (2012) 207–214.

[6] M. Ramar, B. Manikandan, T. Raman, K. Arunagirinathan, N.M. Prabhu, M.J. Basu, M. Perumal, S. Palanisamy, A. Munusamy, Biosynthesis of silver nanoparticles using ethanolic petals extract of *Rosa indica* and characterization of its antibacterial, anticancer and anti-inflammatory activities, Spectrochim. Acta, Part A, 138 (2015) 120–129.

[7] V. Kumar, S. Singh, B. Srivastava, R. Bhadouria, R. Singh, Green synthesis of silver nanoparticles using leaf extract of *Holoptelea integrifolia* and preliminary investigation of its antioxidant, anti-inflammatory, antidiabetic and antibacterial activities, J. Environ. Chem. Eng., 7 (2019) 103094.

[8] T.M. Tolaymat, A.M. El-Badawy, A. Genaidy, K.G. Scheckel, T.P. Luxton, M. Suidan, An evidence-based environmental perspective of manufactured silver nanoparticle in syntheses and applications: a systematic review and critical appraisal of peer-reviewed scientific papers, Sci. Total Environ., 408 (2010) 999–1006.

[9] I. Ghiuta, D. Cristea, C. Croitoru, J. Kost, R. Wenkert, I. Vyrides, A. Anayiotose, D. Munteanu, Characterization and antimicrobial activity of silver nanoparticles biosynthesized using *Bacillus* species, Appl. Surf. Sci., 438 (2018) 66–73.

[10] H. Rostami, F. Khosravi, M. Mohseni, A.A. Rostami, Biosynthesis of Ag nanoparticles using isolated bacteria from contaminated sites and its application as an efficient catalyst for hydrazine electrooxidation, Int. J. Biol. Macromol., 107 (2018) 343–348.

[11] I. Rasaee, M. Ghannadnia, S. Baghshahi, Biosynthesis of silver nanoparticles using leaf extract of *Satureja hortensis* treated with

NaCl and its antibacterial properties, Microporous Mesoporous Mater., 264 (2018) 240–247.
[12] S. Gonçalves, A. Romano, *In vitro* culture of lavenders (*Lavandula* spp.) and the production of secondary metabolites, Biotechnol. Adv., 31 (2013) 166–174.
[13] Y. Li, W. Shen, Morphology-dependent nanocatalysts: rod-shaped oxides, Chem. Soc. Rev., 43 (2014) 1543–1574.
[14] V. Gopinath, D. MubarakAli, S. Priyadarshini, N.M. Priyadharsshini, N. Thajuddin, P. Velusamy, Biosynthesis of silver nanoparticles from *Tribulus terrestris* and its antimicrobial activity: a novel biological approach, Colloids Surf., B, 96 (2012) 69–74.
[15] R.T.V. Vimala, G. Sathishkumar, S. Sivaramakrishnan, Optimization of reaction conditions to fabricate nano-silver using *Couroupita guianensis* Aubl. (Leaf & fruit) and its enhanced larvicidal effect, Spectrochim. Acta, Part A, 135 (2015) 110–115
[16] S. Ahmed, M. Ahmad, B.L. Swami, S. Ikram, A review on plants extract mediated synthesis of silver nanoparticles for antimicrobial applications: a green expertise, J. Adv. Res., 7 (2016) 17–28.
[17] W. Ma, D. Zhong, H. Han, P. Wang, A review: inhibition of Ag NPs on wastewater treatment, Desal. Water Treat., 51 (2013) 7012–7017.
[18] R.F.N. Quadrado, G. Gohlke, R.S. Oliboni, A. Smaniotto, A.R. Fajardo, Hybrid hydrogels containing one-step biosynthesized silver nanoparticles: preparation, characterization and catalytic application, J. Ind. Eng. Chem., 79 (2019) 326–337.
[19] R.W. Raut, N.S. Kolekar, J.R. Lakkakula, V.D. Mendhulkar, S.B. Kashid, Extracellular synthesis of silver nanoparticles using dried leaves of *pongamia pinnata* (L) pierre, Nano Micro Lett., 2 (2010) 106–113.
[20] P. Kuppusamy, S.J.A. Ichwan, N.R. Parine, M.M. Yusoff, G.P. Maniam, N. Govindan, Intracellular biosynthesis of Au and Ag nanoparticles using ethanolic extract of *Brassica oleracea* L. and studies on their physicochemical and biological properties, J. Environ. Sci., 29 (2015) 151–157.
[21] S. Shrivastava, T. Bera, A. Roy, G. Singh, P. Ramachandrarao, D. Dash, Characterization of enhanced antibacterial effects of novel silver nanoparticles, Nanotechnology, 18 (2007) 225103, doi: https://doi.org/10.1088/0957-4484/18/22/225103.
[22] P.D. Shankar, S. Shobana, I. Karuppusamy, A. Pugazhendhi, V.S. Ramkumar, S. Arvindnarayan, G. Kumar, A review on the biosynthesis of metallic nanoparticles (gold and silver) using bio-components of microalgae: formation mechanism and applications, Enzyme Microb. Technol., 95 (2016) 28–44.
[23] O. Zuas, N. Hamim, Y. Sampora, Biosynthesis of silver nanoparticles using water extract of *Myrmecodia pendan* (Sarang Semutplant), Mater. Lett., 123 (2014) 156–159.
[24] S. Pirtarighata, M. Ghannadniab, S. Baghshahi, Biosynthesis of silver nanoparticles using *Ocimum basilicum* cultured under controlled conditions for bactericidal application, Mater. Sci. Eng., C, 98 (2019) 250–255.
[25] M.N. Gallucci, J.C. Fraire, A.P.V.F. Maillard, P.L. Páez, I.M.A. Martínez, E.V.P. Miner, E.A. Coronado, P.R. Dalmasso, Silver nanoparticles from leafy green extract of Belgian endive (*Cichorium intybus* L. var. sativus): biosynthesis, characterization, and antibacterial activity, Mater. Lett., 197 (2017) 98–101.
[26] N.M. Aguilar, F. Arteaga-Cardona, J.O. Estévez, N.R. Silva-González, J.C. Benítez-Serrano, U. Salazar-Kuri, Controlled biosynthesis of silver nanoparticles using sugar industry waste, and its antimicrobial activity, J. Environ. Chem. Eng., 6 (2018) 6275–6281.
[27] P. Kaur, R. Thakur, H. Malwal, A. Manuja, A. Chaudhury, Biosynthesis of biocompatible and recyclable silver/iron and gold/iron core-shell nanoparticles for water purification technology, Biocatal. Agric. Biotechnol., 14 (2018)189–197.
[28] C. Krishnaraj, R. Ramachandran, K. Mohan, P.T. Kalaichelvan, Optimization for rapid synthesis of silver nanoparticles and its effect on phytopathogenic fungi, Spectrochim Acta, Part A, 93 (2012) 95–99.
[29] O.S. Oluwafemi, J.L. Anyik, N.E. Zikalala, E.M. Sakho, Biosynthesis of silver nanoparticles from water hyacinth plant leaves extract for colourimetric sensing of heavy metals, Nano Struct. Nano Objects, 20 (2019) 100387.
[30] M.M. Khalil, E.H. Ismail, F. El-Magdoub, Biosynthesis of Au nanoparticles using olive leaf extract: 1st nano updates, Arabian J. Chem., 5 (2012) 431–437.
[31] P.M. Mishra, S.K. Sahoo, G.K. Naik, K. Parida, Biomimetic synthesis, characterization and mechanism of formation of stable silver nanoparticles using *Averrhoa carambola* L. leaf extract, Mater. Lett., 160 (2015) 566–571.
[32] H. Liu, Y. Sun, H. Zhang, J. Wang, J. Wei, Hydrodynamic cavitation enhanced biosynthesis of silver nanoparticles at room temperature and its mechanism, Mater. Lett., 236 (2019) 387–389.
[33] M.I. Sabela, T. Makhanya, S. Kanchi, M. Shahbaaz, D. Idress, K. Bisetty, One-pot biosynthesis of silver nanoparticles using *Iboza Riparia* and *Ilex Mitis* for cytotoxicity on human embryonic kidney cells, J. Photochem. Photobiol., B, 178 (2018) 560–567.
[34] R.W. Raut, V.D. Mendhulkar, S.B. Kashid, Photosensitized synthesis of silver nanoparticles using *Withania somnifera* leaf powder and silver nitrate, J. Photochem. Photobiol., B, 132 (2014) 45–55.
[35] A.J. Kora, R.B. Sashidhar, J. Arunachalam, Aqueous extract of gum olibanum (*Boswellia serrata*): a reductant and stabilizer for the biosynthesis of antibacterial silver nanoparticles, Process Biochem., 47 (2012) 1516–1520.
[36] D.S. Bharathi, Vasantharaj, V. Bhuvaneshwari, Green synthesis of silver nanoparticles using *Cordia dichotoma* fruit extract and its enhanced antibacterial, anti-biofilm and photo catalytic activity, Mater. Res. Express, 5 (2018) 055404.
[37] J. Du, Z. Hu, W. Dong, Y. Wang, S. Wu, Y. Bai, Biosynthesis of large-sized silver nanoparticles using *Angelica keiskei* extract and its antibacterial activity and mechanisms investigation, Microchem. J., 147 (2019) 333–338.
[38] M. Vanaja, G. Gnanajobitha, K. Paulkumar, S. Rajeshkumar, C. Malarkodi, G. Annadurai, Phytosynthesis of silver nanoparticles by *Cissus quadrangularis*: influence of physicochemical factors, J. Nanostruct. Chem., 3 (2013) 1–8.
[39] O.P. Siwach, P. Sen, Synthesis and study of fluorescence properties of Cu nanoparticles, J. Nanopart. Res., 10 (2008) 107–114.
[40] Z. Jian, Z. Xiang, W. Yongchang, Electrochemical synthesis and fluorescence spectrum properties of silver nanospheres, Microelectron. Eng., 77 (2005) 58–62.
[41] E.I. El-Aswar, M.M. Zahran, M. El-Kemary, Optical and electrochemical studies of silver nanoparticles biosynthesized by *Haplophyllum tuberculatum* extract and their antibacterial activity in wastewater treatment, Mater. Res. Express 6 (2019) 105016.
[42] B. Derjaguin, L. Landau, Theory of the stability of strongly charged lyophobic sols and of the adhesion of strongly charged particles in solutions of electrolytes, Prog. Surf. Sci., 43 (1993) 30–59.
[43] M. El-Kemary, E. Ibrahim, M.F. A-Ajmi, S.A.M. Khalifa, A.D. Alanazi, H.R. El-Seedi, *Calendula officinalis*-mediated biosynthesis of silver nanoparticles and their electrochemical and optical characterization, Int. J. Electrochem. Sci., 11 (2016) 10795–10805.
[44] M. El-Kemary, M. Zahran, S.A.M. Khalifa, H.R. El-Seedi, Spectral characterisation of the silver nanoparticles biosynthesised using *Ambrosia maritima* plant, Micro Nano Lett., 11 (2016) 311–314.
[45] M. Giovanni, M. Pumera, Size dependant electrochemical behavior of silver nanoparticles with sizes of 10, 20, 40, 80 and 107 nm, Electroanalysis, 44 (2012) 615–617.
[46] K. Raja, A. Saravanakumar, R. Vijayakumar, Efficient synthesis of silver nanoparticles from *Prosopis juliflora* leaf extract and its antimicrobial activity using sewage, Spectrochim. Acta, Part A, 97 (2012) 490–494.
[47] I. Sondi, B. Salopek-Sondi, Silver nanoparticles as antimicrobial agent: a case study on *E. coli* as a model for gram-negative bacteria, J. Colloid Interface Sci., 275 (2004) 177–182.
[48] Y.G. Yuan, Q.L. Peng, S. Gurunathan, Effects of silver nanoparticles on multiple drug-resistant strains of *Staphylococcus aureus* and *Pseudomonas aeruginosa* from mastitis-infected goats: an alternative approach for antimicrobial therapy, Int. J. Mol. Sci., 18 (2017) 569.

[49] J. Jeevanandam, A. Barhoum, Y.S. Chan, A. Dufresne, M.K. Danquah, Review on nanoparticles and nanostructured materials: history, sources, toxicity and regulations, Beilstein J. Nanotechnol., 9 (2018) 1050–1074.
[50] S. Valsalam, P. Agastian, M.V. Arasu, N.A. Al-Dhabi, A.M. Ghilan, K. Kaviyarasu, B. Ravindran, S.W. Chang, S. Arokiyaraj, Rapid biosynthesis and characterization of silver nanoparticles from the leaf extract of *Tropaeolum majus* L. and its enhanced *in-vitro* antibacterial, antifungal, antioxidant and anticancer properties, J. Photochem. Photobiol., B, 191 (2019) 65–74.

Supplementary information

Fig. S1a shows the UV-Vis spectra of AgNPs when various concentrations of $AgNO_3$ solution reacted with 10 mL *H. tuberculatum* extract. Increasing of $AgNO_3$ concentration means more silver cations (Ag^+) are progressively bioreduced to (Ag^0) as AgNPs. Absorption peak intensities are almost independent for 3, 4, and 5 mM $AgNO_3$, which means that the reaction is about to reach the equilibrium point as the bioreducing and stabilizing molecules are fully consumed. In this case, it is unattainable to reduce Ag^+ any more. (b) shows the UV-Vis spectra of AgNPs resulted from adding various volumes of plant extract to $AgNO_3$ (3 mM) solution. Due to increasing number of biosynthesized AgNPs, we can observe the growth in absorbance with the increase of *H. tuberculatum* extract concentration. This could attribute to the availability of more bioreducing and stabilizing biomolecules. Absorption peak intensities are almost independent for 17 and 20 mL plant extract, which can be ascribed to absence of Ag^+ in the medium to be bioreduced. (c) displays the UV-Vis spectra related to the kinetics of AgNPs biosynthesis recorded at 2-min intervals for the AgNPs sample resulted from adding 15 mL of plant extract and 100 mL of $AgNO_3$ (3 mM). The SPR band intensities rise as the reaction time is extended up to

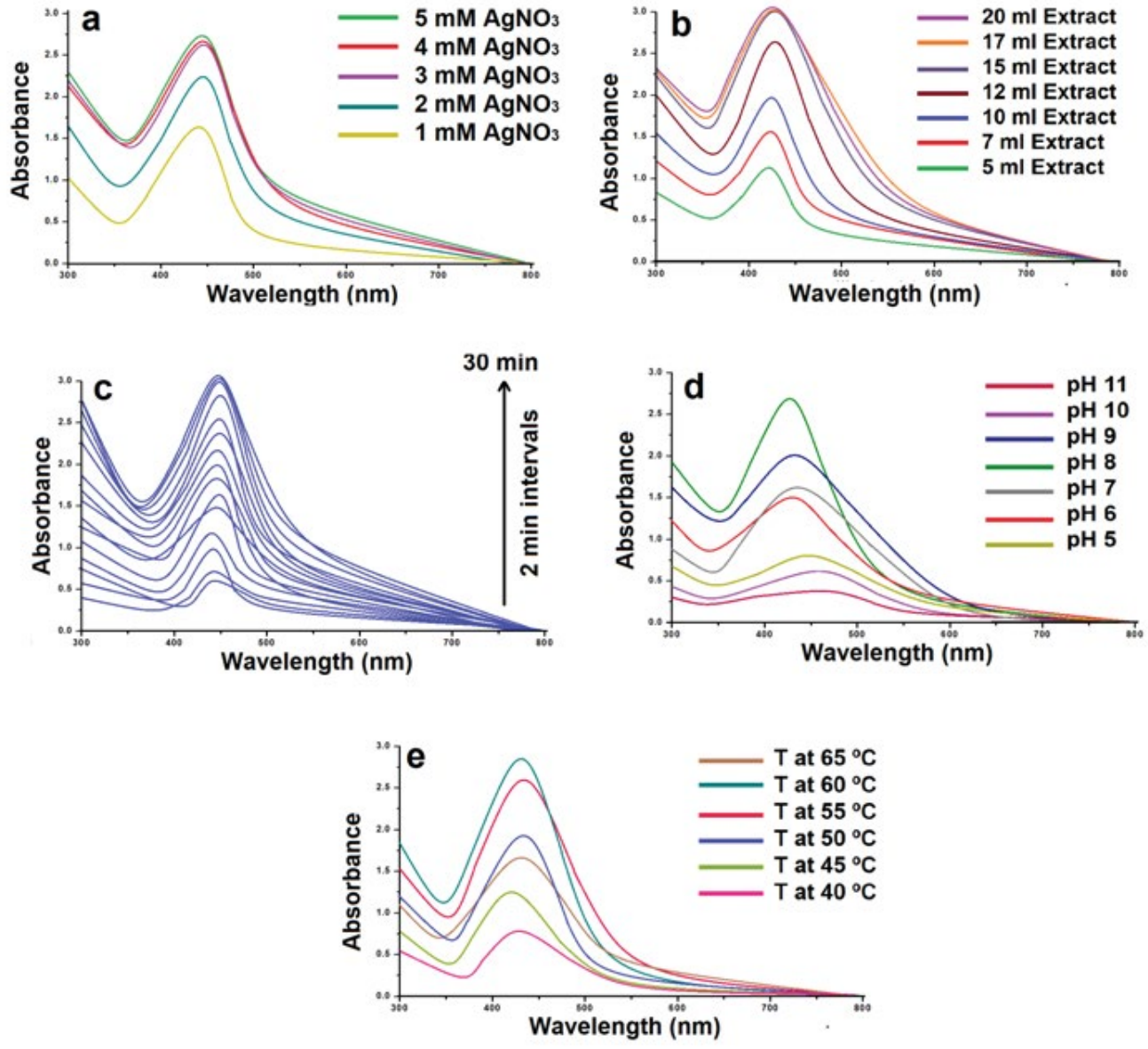

Fig. S1. Effect of silver nitrate (a), plant extract volume (b), reaction time (c), pH (d), reaction temperature (e) on UV-Vis spectra.

30 min. After that time, no cognizable variations in absorbance were observed suggesting that the reaction is at equilibrium. At a neutral medium, the reaction started simultaneously and AgNPs formation was accomplished within 30 min. At acidic pH, the yield of AgNPs was very low and the AgNPs sizes were comparatively larger. At basic pH (7–10), AgNPs yield became high. At pH 11, coagulation of AgNPs was realized. It could be deduced from panel (d) that AgNPs yield increased from pH 5 to pH 8, but the further rise of pH leads to reduction of yield. This reduction may be resulted from increasing aggregations. Increasing the reaction temperature is accompanied with rise in absorbance values, indicating the massive fabrication of AgNPs. The SPR band intensities were improved upon rising in reaction temperature from 40°C to 60°C and afterwards they were declined. According to the panel (e), increasing the temperature higher than 60°C promoted the development of the crystal surrounding the nucleus that may cause absorbance drop.